RSC Mechanochemistry

ROYAL SOCIETY OF CHEMISTRY

PAPER

View Article Online
View Journal | View Issue

Cite this: *RSC Mechanochem.*, 2025, **2**, 544

Solid-state mechanochemical activation of anthracene–maleimide adducts: the influence of the polymer matrix†

Justus P. Wesseler, ‡[a] James R. Hemmer,‡[a] Christoph Weder [a] and José Augusto Berrocal *[ab]

Received 18th February 2025
Accepted 14th April 2025

DOI: 10.1039/d5mr00026b

rsc.li/RSCMechanochem

The repertoire of established mechanophores has been on a steady rise over the last few years, holding the promise of generating materials capable of delivering programmable, beneficial responses upon mechanical stimulation. However, investigations are usually confined to demonstrating activation within limited and seemingly arbitrary choices of polymer matrices. In contrast, the broader applicability of the mechanophore across various types of polymer materials is rarely explored. The experimental techniques generally used to achieve mechanochemical activation are also a source of discrepancy. Ultrasonication of dilute polymer solutions is a popular method that applies extreme strain rates to isolated, solvated chains. The technique is practical and convenient, but its experimental conditions are not conducive to elucidating the activity of the same mechanophore in a bulk polymer system under tensile strain. Here, we report a comparative study on the mechanochemical behaviour of anthracene–maleimide Diels–Alder adducts in a series of polymeric materials. We embed the mechanophores either in the backbone of linear polymers or as cross-links of polymer networks. We show that the solution-phase ultrasonication efficiently activates the mechanophores, regardless of the design of the linear polymer. In contrast, mechanophore activation in bulk is highly dependent on the polymer matrix, topology, and the connectivity of the mechanophore and the matrix.

Introduction

The field of polymer mechanochemistry has flourished over the past two decades thanks to the establishment of the concept of mechanically responsive motives known as mechanophores.[1–3] These rationally designed molecules have provided profound insights into how mechanical forces impact polymer materials and allowed several mechanically triggered responses, including mechanochromism, *i.e.*, changes in polymers' optical properties,[4] the release of small molecules,[5] and the activation of catalytic species,[6] to name but a few.

The activation of covalent mechanophores typically involves the cleavage of intentionally labile chemical bonds under tension and can be achieved in different states of matter, *i.e.*, solutions, gels, and the solid state. Pulsed ultrasonication is generally the method of choice to activate force-responsive systems in solution,[7] while compression or uniaxial elongation are the main methods typically applied for gels and bulk materials.[8,9] These activation strategies can differ significantly in strain rate and other parameters.[10] Additionally, the interactions and dynamics of polymer chains and, thus, their individual and collective response to externally applied mechanical stresses, differ significantly if one compares dilute solutions and solid-state materials.[11] While the outcome of solution experiments provides an initial proof of the mechanochemical viability of a given molecular motif, in bulk polymer materials the force transduction experienced by a mechanophore is highly dependent on the polymer's composition and topology.[12–14] This results in a discrepancy where activation of mechanophores through ultrasonication of dilute solutions is essentially ubiquitous, while the selection of mechanophore, method of mechanophore incorporation, and testing conditions are all important parameters to consider in solid-state experiments.

Several perspectives and reviews have highlighted the role of macromolecular design in controlling the (extent of) mechanochemical activation in solid-state systems.[15–17] Still, a predictive understanding of mechanophore activation in bulk systems has yet to be reached.[13,18] Here, we highlight the facile activation of a mechanophore through pulsed ultrasound in different

[a]*Adolphe Merkle Institute, University of Fribourg, Chemin des Verdiers 4, 1700, Fribourg, Switzerland*

[b]*Institute of Chemical Research of Catalonia (ICIQ), Barcelona Institute of Science and Technology (BIST), Av. Països Catalans, 16, Tarragona, E-43007, Spain. E-mail: jberrocal@iciq.es*

† Electronic supplementary information (ESI) available: Experimental procedures, ^{1}H and ^{13}C NMR spectra of synthesized molecules, evolution of the SEC traces of linear polymers upon increasing exposure to ultrasounds, thermal characterization of all polymer materials, optical fibre fluorescence spectra of stretched samples. See DOI: https://doi.org/10.1039/d5mr00026b

‡ Equal contribution from these authors.

polymer backbones and contrast this with bulk tensile studies on the mechanochemical activation of the same mechanophore incorporated into different polymer matrices. In the bulk studies, we embed the mechanophore within tough thermoplastics and elastomers, either within the backbone of linear chains or as cross-links in polymer networks, to provide a broad range of mechanical properties to compare the solution studies to. Additionally, we probe how the variations in stress accumulation can affect mechanophore activation by comparing linear and cross-linked systems.

Within the repertoire of established mechanophores, numerous Diels–Alder (DA) adducts have been shown to undergo force-induced retro-cycloadditions.[4,16,19] These include maleimide–furan (**MF**),[20–24] maleimide–cyclopentadiene (**MC**),[19,25] furan–acetylene,[26] and maleimide–anthracene (**AM**; Fig. 1) adducts.[27–39] Investigations probing DA mechanophores' designs have revealed a strong dependence on the regiochemistry of polymer attachment.[20,24] These DA-adduct mechanophores have been used to fabricate mechanically responsive materials, in which **MF** and **MC** adducts were shown to promote force-induced small molecule release[21,40] and unmasking of photoswitches.[19,25]

The mechanochemical susceptibility of anthracene–maleimide DA adducts (**AM**) was first reported in 2014.[31] The mechanical stimulation of judiciously designed macromolecules that contain such **AM** motifs can trigger the retro-[4 + 2] cycloaddition, affording the anthracene and maleimide constituents (Fig. 1).[15] The process can be conveniently monitored by fluorescence spectroscopy, as anthracene is emissive, while the DA adduct is not fluorescent.

Following the establishment of **AM** adducts as mechanophores, derivatives featuring aromatic extensions in the 9-position of the anthracene, namely 9-π-extended anthracene **AM** adducts, were rapidly developed.[37] This structural variation allowed the design of **AM** mechanophores with red-shifted absorption/emission and higher fluorescence quantum yields. Further developments of 9-π-extended anthracene **AM** adducts also enabled dual-fluorescent optical force probes, in which the non-activated **AM** adduct is also fluorescent, and the fluorescence readout is facilitated by the large spectral separation due to the bathochromically shifted emission of the 9-π-extended anthracene.[35,38,41] The drastic change in the optical properties accompanying the force-induced scission of such 9-π-extended anthracene **AM** adducts facilitated locally resolved, quantitative damage detection by confocal laser scanning microscopy.[38,41] Furthermore, the improved quantum yield and higher resistance to photobleaching have made the 9-π-extended **AM** mechanophores a popular choice, with numerous investigations involving the 9-π-extended anthracene derivatives generating mechanoresponsive solid materials.[27,28,30,36,39,42] These derivatives have been shown to activate in various poly(meth)acrylate-based networks, epoxy resin composites, and poly(*N*-isopropylacrylamide) hydrogels successfully when incorporated as cross-links.[27,28,30,36,39,42] On the other hand, the mechanochemistry of **AM** motifs that do not comprise 9-π-extended anthracenes, hereafter referred to as non-π-extended **AM**, has been extensively explored in solutions and at the interface between polymer brushes and surfaces.[16,43–46] In contrast, only a few studies have been dedicated to the mechanochemical activation of these motifs in solid-state polymers.[32,34,47] One investigation disclosed the release of anthracene due to compressive forces on poly(*N*,*N*-dimethylacrylamide) networks cross-linked by non-π-extended **AM** units.[32] Laser-induced stress waves have been used to activate non-π-extended **AM** units bonded between silica–epoxy interfaces,[34] while manual grinding of poly(norbornene)-*graft*-poly(styrene) was used to cleave non-π-extended **AM** units at backbone-arm junctions.[47]

The wealth of force-sensitive systems investigated incorporating the **AM** motif led our curiosity to embark on the study presented here. Consequently, we compare the mechanochemical activation of the **AM** unit (*i.e.*, non-π-extended) in four different polymer matrices to investigate how the nature of the polymer matrix and mechanophore location affect the activation of this particular **AM** mechanophore.

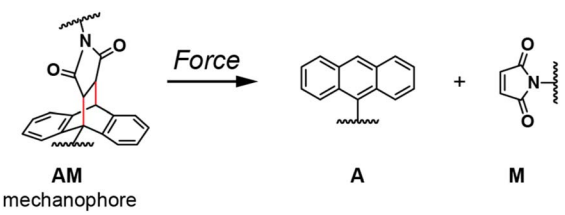

Fig. 1 Force-assisted retro-[4 + 2] cycloaddition of AM adducts.

Results and discussion

Synthesis of the small molecule mechanophores and their incorporation into polymers

We started our investigation by synthesising non-π-extended **AM-1**, **AM-2**, **AM-3**, and **AM-4**, which are based on the basic skeleton of the anthracene–maleimide adduct (Fig. 2a–d). We kept the core of the molecular design of **AM-1/2/3/4** consistent and decorated it with judiciously chosen functional groups to allow the incorporation of these **AM** derivatives into a series of polymer matrices.

Diol **AM-1** (ref. 32) afforded polyurethane **PU$_L$-AM-1** upon reaction with butanediol, methylene diphenyl diisocyanate (MDI), poly(tetrahydrofuran) (PTHF), and dibutyltin dilaurate (DBTL) (Fig. 2a). The polymer made had a number-average molecular weight (M_n) of 123 kg mol^{-1}, a dispersity ($Đ$) of 2.24, and a mechanophore concentration of 0.014 mmol of **AM-1** units per gram of polymer (0.014 mmol g^{-1}), which translates into an average of 1.1 mechanophores per chain molecule (*ca.* 0.62 mol%). The nature of the polymerisation reaction (step-growth) causes the mechanophores to be incorporated statistically anywhere along the polymer chains. Thus, the cartoon of **PU$_L$-AM-1** shown in Fig. 2a represents only one of the many possible configurations synthesised. Compound **AM-2**, equipped with two α-bromoisobutyryl groups, served as a bifunctional initiator for the Cu(0)-catalysed atom transfer radical polymerisation (ATRP) of methyl acrylate (MA),[48] which afforded linear poly(methyl acrylate) **PMA$_L$-AM-2** with M_n = 99.5 kg

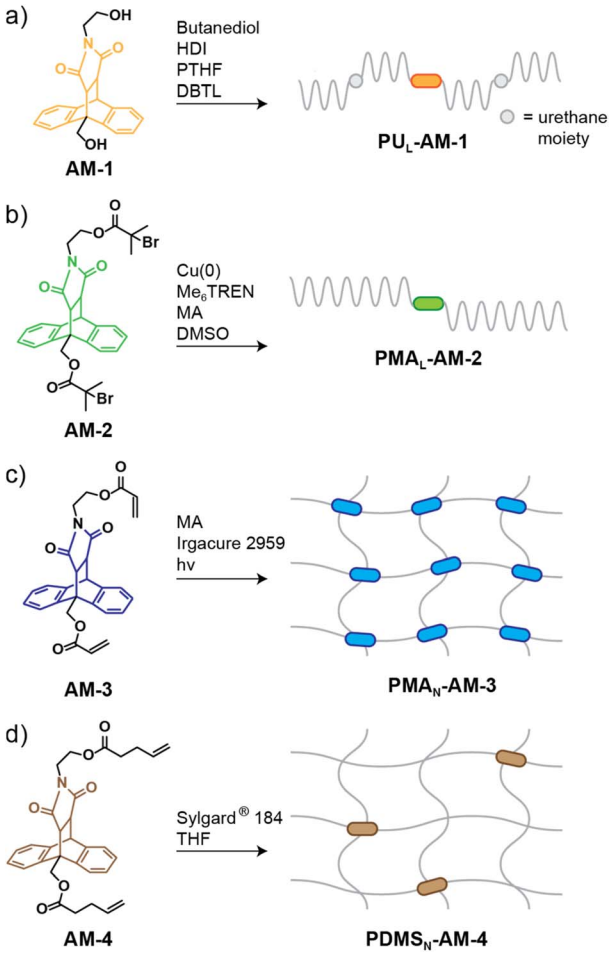

Fig. 2 Chemical structures and synthetic strategies used for the preparation of (a) AM-1 and PU$_L$-AM-1 (the cartoon represents only one of the many configurations synthesised), (b) AM-2 and PMA$_L$-AM-2, (c) AM-3 and PMA$_N$-AM-3, and (d) AM-4 and PDMS$_N$-AM-4.

mol^{-1} and $Đ = 1.23$ (Fig. 2b). The polymer chains contain one **AM-2** residue in the central region of the chain, corresponding to an **AM-2** content of 0.018 mmol g^{-1} (*ca.* 0.63 mol%). We employed **AM-3**, functionalised with two acrylate groups, as a cross-linker in the photopolymerisation of MA to produce poly(methyl acrylate) networks **PMA$_N$-AM-3** (Fig. 2c). The density of **AM-3** cross-links in the final material was 0.014 mmol g^{-1} to mirror the loading of **AM-2** in **PMA$_L$-AM-2** (*ca.* 1.2 mol%). Finally, the bifunctional terminal-olefin-bearing **AM-4** enabled the preparation of poly(dimethylsiloxane) (PDMS) network **PDMS$_N$-AM-4** *via* the hydrosilylation of the commercially available Sylgard® 184 silicone elastomer kit (Fig. 2d). Note that **AM-4** was used as an auxiliary cross-linker in **PDMS$_N$-AM-4**, while **AM-3** was the only cross-linker in **PMA$_N$-AM-3**. The mechanophore loading of **PDMS$_N$-AM-4** was 0.014 mmol g^{-1}, similar to the other materials, and the material was cured in the shape of films. To verify the inclusion of **AM-4** in the PDMS network, a strip of the film was soaked in THF overnight. The resulting THF solution was dried *in vacuo* and redissolved in $CDCl_3$ to be analysed by ^{1}H NMR spectroscopy. The ^{1}H NMR spectrum revealed just the presence of solvents and some soluble PDMS fraction, suggesting that the entire feed of **AM-4** was covalently incorporated in **PDMS$_N$-AM-4** (Fig. S3†). The synthetic procedures and characterisation of **AM-1/2/3/4** and related polymer systems can be found in the ESI (pages S4–S7†).

Evaluation of the mechanochemical reactivity in linear polymers

We first evaluated the mechanochemical reactivity of our **AM** mechanophores embedded in the linear polymers, starting with the ultrasonication of dilute (2 mg mL^{-1}) THF solutions of **PU$_L$-AM-1** and **PMA$_L$-AM-2**. The solutions were subjected to pulses (1 s on, 1 s off) of 20 kHz ultrasound for a total of 2.5 hours of effective sonication time while being kept in an ice bath. At regular time intervals, aliquots (1 mL) of the solutions were analysed by fluorescence spectroscopy and size exclusion chromatography (SEC). The fluorescence spectra ($\lambda_{ex} = 350$ nm) of ultrasonicated aliquot solutions of **PU$_L$-AM-1** and **PMA$_L$-AM-2** were recorded and compared to those acquired for solutions of the untreated polymers (Fig. 3a and b). The emission of the ultrasonicated solutions (Fig. 3) shows the characteristic profile of the released anthracene species, with emission maxima at 390, 412, and 436 nm, as previously reported for other non-π-extended **AM**-based systems.[32,43]

To obtain further insights into the ultrasound-assisted scission of the **AM** adduct, we monitored the polymer fractioning as a function of sonication time by SEC analysis. For **PU$_L$-AM-1**, ultrasound treatment resulted in the continuous scission of the starting polymer (M_n = 123 kg mol^{-1}) to lower M_n values and reached a value of 65 kg mol^{-1} after 150 min (Fig. 4a and S5†). In the case of **PMA$_L$-AM-2** (M_n = 100 kg mol^{-1}), ultrasound-induced scission of the **AM** mechanophore was expected to

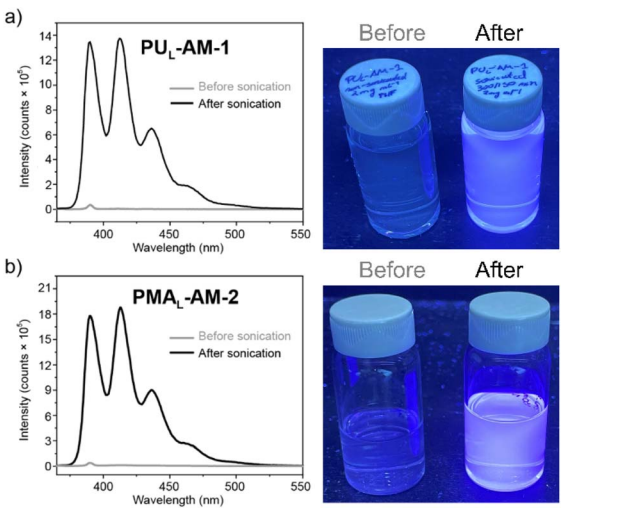

Fig. 3 Fluorescence spectra (λ_{ex} = 350 nm) of solutions of (a) PU$_L$-AM-1 and (b) PMA$_L$-AM-2 in THF (concentration = 2 mg mL^{-1}) before (grey line) and after (black line) ultrasound treatment (150 minutes, 10% amplitude, max power 400 W). The photographs show the polymer solutions before and after ultrasound treatment under irradiation with UV light (λ_{ex} = 365 nm).

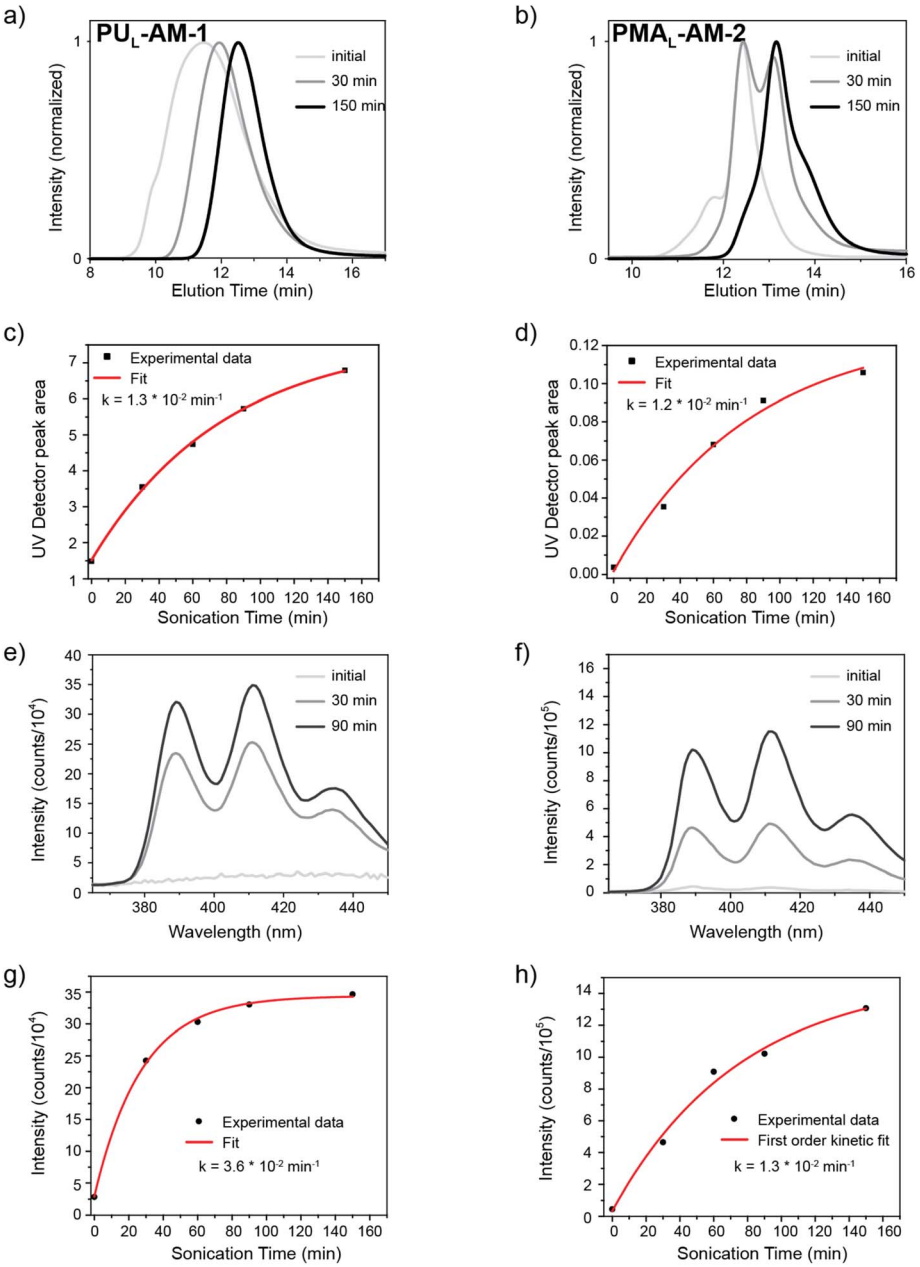

Fig. 4 (a) Normalized SEC traces (RID) of **PU$_L$-AM-1** measured at time zero, and after 30 and 150 min of effective sonication time. (b) Normalized SEC traces (RID) of **PMA$_L$-AM-2** measured at time zero, and after 30 and 150 min of effective sonication time. (c) Plot of integrated peak area (λ = 347 nm) against effective sonication time as measured by the VWD detector during SEC analysis for **PU$_L$-AM-1** and first-order kinetics fit. Minor absorbance originating from the polyurethane results in the absorbance value of t_0 being non-zero. (d) Plot of integrated peak area (λ = 254 nm) against effective sonication time as measured by the VWD detector during SEC analysis for **PMA$_L$-AM-2** and first-order kinetics fit. (e) Fluorescence spectra of **PU$_L$-AM-1** aliquots at different effective sonication times. (f) Fluorescence spectra of **PMA$_L$-AM-2** aliquots at different effective sonication times. (g) Plot of fluorescence intensity (λ_{em} = 390 nm) against sonication time for **PU$_L$-AM-1** and first-order kinetics fit. (h) Plot of fluorescence intensity (λ_{em} = 390 nm) against sonication time for **PMA$_L$-AM-2** and first-order kinetics fit.

yield new species whose M_n values correspond to roughly half of the original polymers due to the placement of the mechanophores in the central region of each chain (Fig. 4b). The shoulder of the main peak in the SEC trace of **PMA$_L$-AM-2**, which appears at 11.8 min, is due to bimolecular termination during ATRP (Fig. 4b). After 30 minutes of sonication, a bimodal trace with a lower molecular weight peak corresponding to a newly formed species of approximately 48 kg mol^{-1} was observed (Fig. 4b). This is accompanied by the disappearance of the shoulder peak initially observed at 11.8 min (Fig. 4b). Further sonication time points at 60, 90, and 150 minutes for **PMA$_L$-AM-2** revealed continuous growth of the peak associated with the reduced M_n of *ca.* 48 kg mol^{-1} and a concomitant decrease of the peak centred around 100 kg mol^{-1} (Fig. S5†). In

addition, a weak, shoulder peak associated with lower M_n species emerges with increased sonication time, which suggests that the chains can be cleaved again, albeit with lower efficiency and certainly in a process that does not involve the mechanophores, which after the first cleavage must be located near the ends of the polymer chains (Fig. 4b and S5†).

It was also possible to monitor the **AM** cleavage as a function of sonication time using the UV detector of the SEC instrument (Fig. S5†), which can be set at a pre-determined wavelength. In the case of **PU_L-AM-1**, the absorbance was monitored at 347 nm, where the anthracene exhibits an absorbance peak, and the polyurethane has a negligible absorption. In the case of **PMA_L-AM-2**, the absorbance was measured at 254 nm, as the unsonicated polymer has negligible absorbance at this wavelength. The UV detector's SEC trace of **PMA_L-AM-2** taken before sonication shows a feint anthracene absorbance, possibly due to a minor amount of degraded **AM**-adducts before sonication. The fraction of these species was determined to be 1.7 mol% (*vide infra*), and this value was subtracted from the percentage of activated **AM** units in subsequent timepoints. We did not observe any evolution of anthracene spectroscopically during the sonication of small molecule **AM-4** (Fig. S6†), and therefore attribute the increasing absorbance/fluorescence of sonicated **PMA_L-AM-2** to the mechanochemical processes alone. First-order kinetic profiles were evident from the evolution of the anthracene absorbance in both systems (Fig. 4c and d). The rate constants for the retro-DA reaction were determined by fitting the integrated areas of the chromatograms from the SEC's UV detector against sonication time to a first-order kinetics equation (eqn (1))

$$A_t = A_0 + A(1 - e^{-kt}) \quad (1)$$

where A_t is the absorbance peak area of the cleaved polymer at time t, A_0 is the absorbance peak area of the unsonicated polymer, A is the maximum absorbance peak area, and k is the rate constant (Fig. 4c). The calculated rate constants for **PU_L-AM-1** and **PMA_L-AM-2** were 1.3×10^{-2} min^{-1} and 1.2×10^{-2} min^{-1}, respectively.

Building on these results, it was possible to gain further insights into the degree of **AM** activation in **PU_L-AM-1** and **PMA_L-AM-2** by conventional UV-vis absorption spectroscopy, using a calibration curve that was built from solutions of known anthracene concentrations. The latter provided the amount of activated **AM** (or liberated anthracene) within the final aliquot of the sonication experiment (page S9†). For **PU_L-AM-1**, **AM** activation reached *ca.* 22% after 150 minutes of effective sonication time (Fig. S6†). For **PMA_L-AM-2**, it was possible to determine the extent of **AM** activation using the methods previously described by Diesendruck and coworkers.[49] Thus, an **AM** activation of 50 mol% after sonication for 150 minutes was determined (Fig. S7 and S8†). ^{1}H NMR analysis of the final timepoint provided a value of *ca.* 47 mol%, corroborating the degree of **AM** activation determined by UV-vis (Fig. S4†). The random distribution of **AM** units within the backbone of **PU_L-AM-1** evidently impacts mechanophore activation compared to **PMA_L-AM-2**, where the mechanophore is highly localised at the chain centre. It should also be noted that the higher molecular weight shoulder seen at the 30 minutes timepoint SEC trace (UV detector) of **PMA_L-AM-2** is more likely to arise from **AM**-activation in the polymer chains, which underwent bimolecular termination during synthesis (Fig. S5b†).

Additionally, we monitored the outcome of the sonication experiments by fluorescence spectroscopy (Fig. 4e and f for **PU_L-AM-1** and **PMA_L-AM-2**, respectively). The aliquots taken during the sonication experiments were directly transferred to fluorescence cuvettes. The intensity of anthracene fluorescence increased with sonication time for both **PU_L-AM-1** and **PMA_L-AM-2** (Fig. 4e and f). Plotting the fluorescence intensity at 390 nm against the effective sonication time reflect again that the **AM** activation fits a first-order kinetic profile for **PU_L-AM-1** and **PMA_L-AM-2** (Fig. 4g and h, respectively). Such fluorescence profiles contrast starkly with the absence of appreciable fluorescence in the untreated solutions of **PU_L-AM-1**. Once more, the feint anthracene fluorescence could be observed for the untreated **PMA_L-AM-2** solution. Using eqn (1) (replacing absorbance for fluorescence intensity), fluorescence spectroscopy yielded rate constants of 3.6×10^{-2} min^{-1} and 1.3×10^{-2} min^{-1} for **PU_L-AM-1** and **PMA_L-AM-2**. In both cases, *i.e.*, fitting the absorbance and fluorescence data, the rate constant determined for **PU_L-AM-1** was higher than that of **PMA_L-AM-2**. The maximum evolution of anthracene is likely reached faster for **PU_L-AM-1** over **PMA_L-AM-2** due to a higher occurrence of non-selective scissile events in the former polymer.[50] However, the specific chain-centred location of **AM** units in **PMA_L-AM-2** results in a significant increase in overall mechanophore activation efficiency.

Evaluation of the mechanochemical reactivity in solid-state polymers

Having established the mechanochemical activity of the **AM** motifs in our linear polymer systems by exposure to pulsed ultrasounds, we investigated the mechanoresponse of **AM-1** to **AM-4** embedded in solid polymer matrices. Films of the four polymers with a thickness of between 180 and 300 μm were prepared following different procedures. The linear polymers **PU_L-AM-1** and **PMA_L-AM-2** were solvent-cast from THF solutions into poly(tetrafluoroethylene) (PTFE) Petri dishes. This was followed by air- and subsequently vacuum-drying overnight at room temperature. Films of **PU_L-AM-1** were then cut into dogbone-shaped specimens due to the high tensile strength of this material, while **PMA_L-AM-2** films were cut into rectangular strips. The cross-linked **PMA_N-AM-3** samples were prepared by performing the photopolymerisation (*cf.* Fig. 2d) between glass slides, air drying the resulting films, and cutting them into rectangular strips. Finally, **$PDMS_N$-AM-4** was prepared by polymerisation (*cf.* Fig. 2e) in PTFE dishes, air drying the obtained material, and cutting the films thus made into rectangular strips.

Besides the positioning of the mechanophore's functional handles for incorporation into polymers, which was the same for all materials investigated here, effective force transduction onto mechanophores in solid materials depends on the

material's inherent properties, such as its glass transition temperature (T_g) and viscoelasticity.[51] Thus, we characterised the thermal properties of the four polymers by differential scanning calorimetry (DSC). From the DSC data of **PU$_L$-AM-1**, the soft segments were determined to have a T_g of *ca.* −71 °C, while the hard segments had a T_m of *ca.* 190 °C (Fig. S9†). This demonstrates that in **PU$_L$-AM-1**, the **AM** motif sits in a phase-segregated host matrix. The absence of any other transition in the DSC traces of **PMA$_L$-AM-2**, **PMA$_N$-AM-3**, and **PDMS$_N$-AM-4**, other than the T_g at *ca.* 13 and 17 °C for **PMA$_L$-AM-2** and **PMA$_N$-AM-3**, respectively, reflects that these polymers are amorphous (Fig. S10–S12†).

Tensile tests carried out on films of **PU$_L$-AM-1**, **PMA$_L$-AM-2**, **PMA$_N$-AM-3**, and **PDMS$_N$-AM-4** reveal that the mechanical properties of the four polymer materials cover a broad range (Fig. 5a and Table S1†). On account of its microphase-separated morphology and the high density of physical cross-links, **PU$_L$-AM-1** is the stiffest and toughest material, exhibiting a tensile strength (σ_B) of 58 MPa, and a strain at break (ε_B) of 762% (Fig. 5a, orange line). Due to its low T_g and the absence of any cross-links other than entanglements, **PMA$_L$-AM-2** is much softer (σ_B = 0.59 MPa) yet highly deformable (ε_B = 1778%) (Fig. 5a, green line). The stress–strain curve of the cross-linked **PMA$_N$-AM-3** falls in between those of **PU$_L$-AM-1** and **PMA$_L$-AM-2**, and reflects σ_B = 19 MPa, and ε_B = 773% (Fig. 5a, blue line). **PDMS$_N$-AM-4** proved to be much weaker, with σ_B = 3.7 MPa and ε_B = 127% (Fig. 5a, purple line), values similar to previous reports of PDMS networks produced from Sylgard® 184.[52,53] The inflexion observed for **PMA$_N$-AM-3** at $\sigma \approx 12.5$ MPa and $\varepsilon \approx$ 485% is accompanied by the onset of opaqueness of the materials and attributed to strain-induced crystallisation.

To investigate how the different molecular topologies and mechanical properties of the four polymers affect the mechanochemical activation of the **AM** units, the polymer samples were deformed by uniaxial elongation at a strain rate of 125% min^{-1} (=50 mm min^{-1}) to failure, and their emission was qualitatively assessed by visually comparing the films before and after deformation upon irradiation with 365 nm light (Fig. 5b). Neither of the materials shows any appreciable fluorescence in the as-prepared state, which reflects that the mechanophores are not activated during processing. Interestingly, only **PMA$_N$-AM-3** shows a clear fluorescence change upon mechanical deformation. The sample was non-emissive before applying force, but a blue emission reminiscent of the colour observed for the corresponding ultrasonicated solution shown in Fig. 2 was detected (Fig. 5b). The post-mortem picture shows that the emission developed only in the region of the sample that was not clamped, *i.e.*, in the part that had been strained. Under UV light, the **PMA$_L$-AM-2** samples appear somewhat brighter than the **PU$_L$-AM-1** and **PDMS$_N$-AM-4** films, possibly due to small amounts of residual copper complex impurities from the ATRP polymerisation. The latter are highly emissive, although they are present in traces.

Steady-state fluorescence measurements on the ruptured samples confirmed the qualitative results discussed above (Fig. 5c). *In situ* fluorescence measurements of solid, as-prepared, and uniaxially deformed polymer samples were measured using an optical fibre setup. The fluorescence spectra

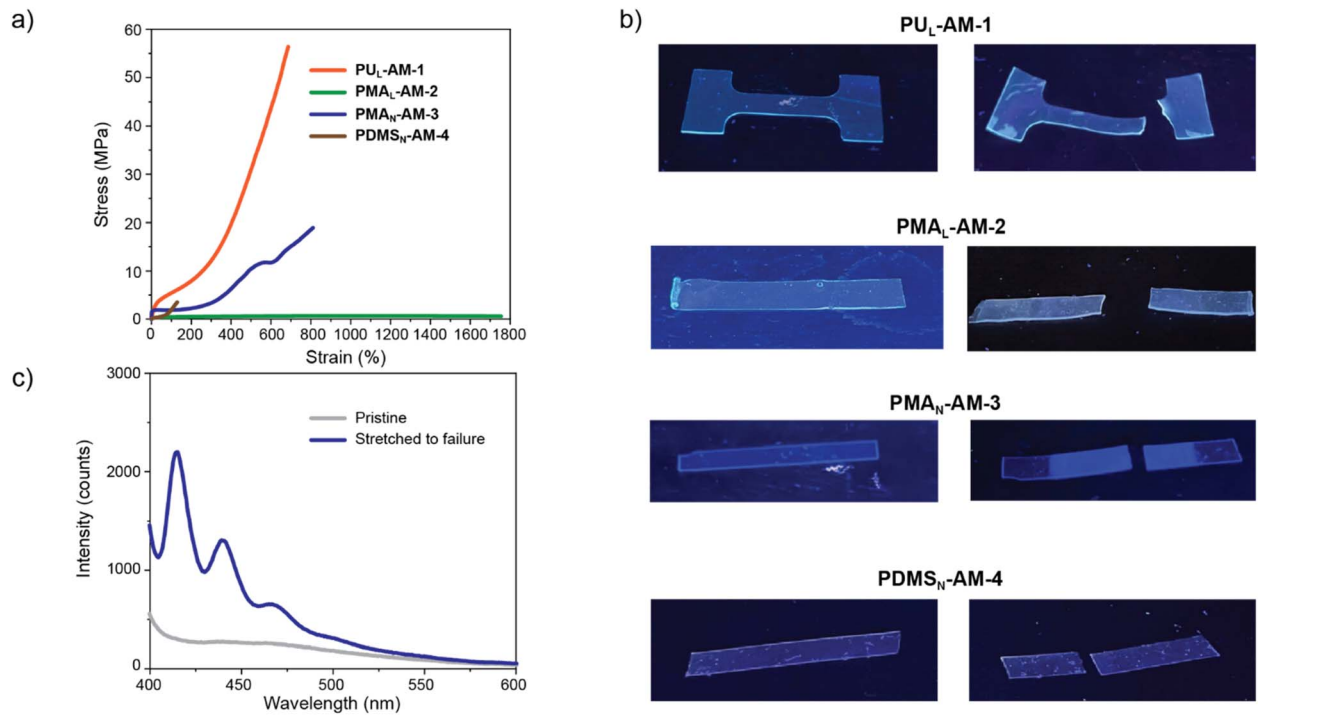

Fig. 5 (a) Stress–strain curves of the studied AM-containing polymer systems. (b) Photographs of AM-containing polymers before and after tensile extension until failure (films placed in a black box and illuminated with 365 nm light). (c) Fluorescence spectra (λ_{ex} = 350 nm) of a PMA$_N$-AM-3 film before and after uniaxial elongation to failure.

of **PU_L-AM-1**, **PMA_L-AM-2**, and **$PDMS_N$-AM-4** are featureless and do not display significant changes upon deformation (Fig. S17–S19†). In contrast, the characteristic emission spectrum of anthracene – albeit slightly red-shifted and perturbed with respect to the fluorescence spectrum of the corresponding ultrasonicated solution (Fig. 3) – was observed for the mechanically deformed **PMA_N-AM-3** (Fig. 5c). The data reflects that the activation of the **AM** mechanophore differs considerably if one compares solution and solid-state experiments. In solution, the **AM** mechanophore activation is highly effective upon the application of ultrasonication, while the widespread activation of **AM** in the solid state could only be achieved in the case of **PMA_N-AM-3**, where the mechanophore motif is used as the exclusive cross-linking species within a host polymer matrix able to withstand significant stresses and strain.

As previously mentioned, one of the crucial differences between ultrasonication of dilute solutions and bulk elongation of solid films is the strain rate experienced by the polymer chains. The cavitation phenomena occurring during ultrasonication result in hydrodynamic forces producing strain rates that are multiple orders of magnitude larger than what is generally accessible with tensile testing machines.[10] Besides appropriate strain rates, the applied stress must exceed the bond's tensile strength and be applied within a time frame less than the vibration period of the bond to produce the mechanical bond scission.[54] Previous reports have demonstrated an increased mechanophore activation rate with increased strain rate.[55,56] Consequently, we were intrigued to see if significantly increasing the strain rate during the elongation of our bulk films could potentially lead to noticeable **AM** activation of the samples that had not shown any activity in the experiments shown in Fig. 5. **PU_L-AM-1**, **PMA_L-AM-2** and **$PDMS_N$-AM-4** films were stretched until failure at strain rates of 2500% min^{-1} and 5000% min^{-1} (Fig. 6a). We noticed drastic differences between the mechanical properties of the same polymers under these new experimental conditions (compare Fig. 5a and 6a). This was expected, as the tensile properties of polymers are sensitive to the applied strain rate.[57]

Indeed, the stress–strain curves of **PMA_L-AM-2** showed well-defined elastic and strain-hardening regions (Fig. 6a), which are absent in the stress–strain curve shown in Fig. 5a. Moreover, ε_B decreased to 770% (2500% min^{-1}) and 510% (5000% min^{-1}), while σ_B significantly increased to 9 MPa (2500% min^{-1}) and 6.3 MPa (5000% min^{-1}). The increased strain rates resulted in lowering σ_B to 24.6 MPa and 19.9 MPa for 2500% min^{-1} and 5000% min^{-1} for **PU_L-AM-1**, respectively, with relatively similar ε_B (Fig. 6a). The mechanical properties of **$PDMS_N$-AM-4** remained relatively unaffected at these strain rates (Fig. 6a).

Despite these drastic changes in tensile properties, we observed no distinct fluorescence in the stretched regions of these samples (Fig. 6c). Examining the fractured films using the optical fibre setup near the point of fracture revealed the activation of **AM** motifs in **PMA_L-AM-2** (Fig. 6b). However, such activation is challenging to interpret due to the small cross-section of the film, the limited area in which it can be measured, and the variations in the distance of the optical fibre probe from the sample during hand-held measurements. The

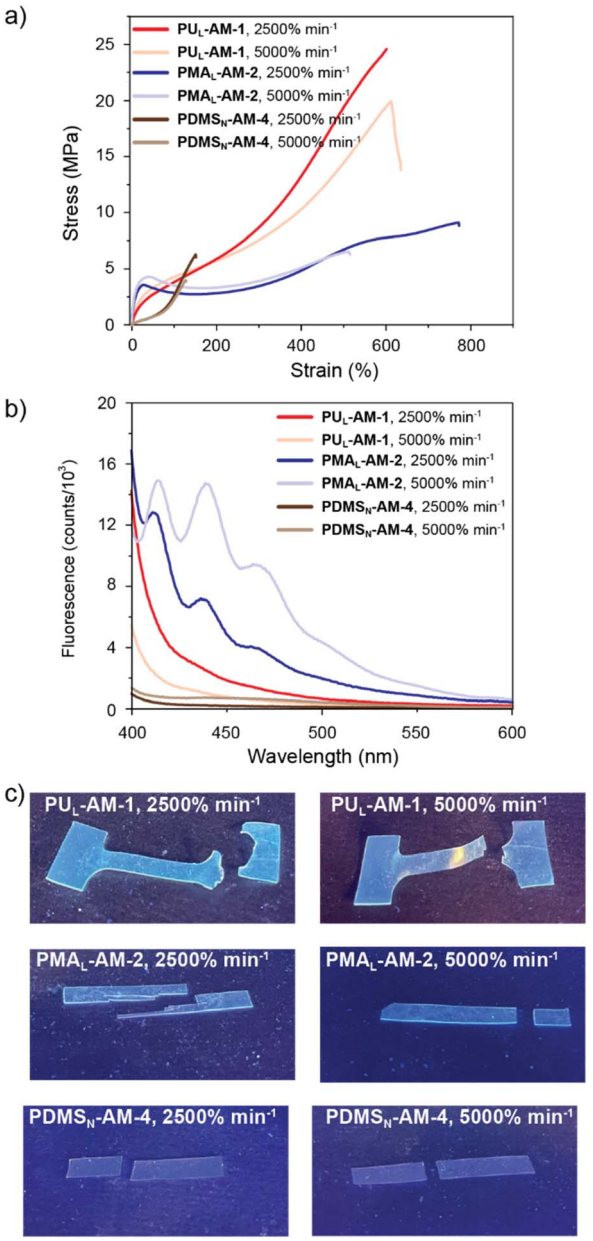

Fig. 6 (a) Stress–strain curves of **PU_L-AM-1**, **PMA_L-AM-2**, and **$PDMS_N$-AM-4** measured at strain rates of 2500% min^{-1} and 5000% min^{-1}. (b) Fluorescence spectra (λ_{ex} = 350 nm) of **PU_L-AM-1**, **PMA_L-AM-2**, and **$PDMS_N$-AM-4** films after uniaxial elongation to failure at strain rates of 2500% min^{-1} and 5000% min^{-1}. (c) Photographs of **PU_L-AM-1**, **PMA_L-AM-2**, and **$PDMS_N$-AM-4** after uniaxial elongation to failure at high strain rate (films placed in a black box and illuminated with 365 nm light).

localisation of the **AM** activation near the fracture point in **PMA_L-AM-2** is congruent with existing reports of other non-π-extended **AM** and 9-π-extended **AM** mechanophores used as cross-links in glassy (meth)acrylate and acrylamide networks.[32,36,38,39,41] This feature has previously allowed for quantitative measurement of broken cross-links at rupture sites of these glassy polymers by confocal microscopy.[38]

Discussion on the mechanochemical reactivity of the AM mechanophores in the four solid-state polymer systems

It is generally known that the activation of covalent mechanophores in solid-state matrices requires the force-responsive species to experience a combination of relatively high stress and strain. Additionally, polymer topology and location of the mechanophore in the architectures are crucial for successful activation in solid-state polymers.[58] For example, tensile elongation of cross-linked materials concentrates stress on the cross-links, which prevent chains from sliding past each other. It follows that the retro-cycloaddition of the **AM** motifs is a favoured stress dissipation mechanism throughout the elongated regions of **PMA$_N$-AM-3**, which is solely cross-linked by **AM** units. In contrast, the areas held in the clamps remain unaffected.

The lack of **AM** activation in **PDMS$_N$-AM-4** is possibly due to the lower tensile strength of PDMS, which results in insufficient stress accumulation at the level of the cross-links before failure of the material. The lack of evident **AM** activation may further be exacerbated in the PDMS system due to competing scission of non-functional cross-link units. Previous reports on PDMS-based systems featuring phenyltriazolinedione–anthracene adducts as cross-links disclosed that the force-modulated liberation of anthracene could only be triggered at very high temperatures (175 °C),[8] suggesting that in a weak polymer matrix such as PDMS, the combination of mechanical force and thermal energy at room temperature does not suffice to overcome the activation barrier for such retro-cycloadditions. Nevertheless, alternative PDMS network designs solely relying on **AM** units as cross-links ought to concentrate internal stresses on **AM** units exclusively and thus yield mechanophore activation. Spiropyran, dioxetane, and rhodamine mechanophores have also been shown to activate in interpenetrated double- or triple-network elastomers.[59–62] While such approaches reduce the onset strain for activation, it should be mentioned that the critical stress of activation for these mechanophores is significantly lower than that of **AM**.[16] Moreover, certain triple networks are capable of reaching σ_B values of up to 29 MPa.[60] It follows that material design plays a crucial role in optimizing mechanophore activation in elastomers.

In the case of linear elastomeric polymer materials such as **PMA$_L$-AM-2**, stress transfer between chains is based on chain disentanglement; the mechanical stress is not explicitly concentrated on the **AM** motifs during chain elongation, which explains the lack of mechanochemical activation. Previous studies on spiropyran-containing triblock copolymers have demonstrated that microphase separation was beneficial in enhancing mechanophore activation, as it resulted in the formation of physical cross-links.[51] A similar strategy could lead to solid-state **AM** activation in linear polyacrylates, although the previous studies used mechanophores that (i) already activated in simple linear acrylates and (ii) had lower force activation thresholds.[51]

The composition of soft and hard segments of **PU$_L$-AM-1** makes it challenging to establish fair comparisons with the other amorphous systems. This case study is intriguing also because of the mechanical properties of the material, which is by far the strongest and the toughest of the scope that we investigated. Based on these properties, one might have predicted *a priori* an easy activation of the **AM** motifs in this matrix, yet our experiments document the opposite. Polyurethanes experiencing tensile stress can be considered to undergo multiple distinct processes,[55,63] with preferential orientation of domains occurring at low strains[64] and phase-mixing followed by alignment of segments at higher elongations. The onset of activation of covalent mechanophores in polyurethanes typically occurs within the strain hardening region, indicating that a high degree of chain alignment along the tensile stress direction is a prerequisite.[65] Mechanophores are generally introduced within the soft segments of polyurethanes.[66,67] Thus, their activation is favoured by the alignment of the soft segments in the direction of the applied tensile stress. Nonetheless, spiropyran and dioxetane mechanophores have also been included in the hard segment of polyurethanes,[55,68] and these studies revealed similar levels of activation compared to soft segment inclusion, albeit with a lower degree of mechanophore alignment to the tensile stress direction.[68] The case of 1,2-dioxetane mechanophores is intriguing, as they have similar force threshold values to **AM**.[15,55] The difference between our system and that of 1,2-dioxetanes[55] is in the composition and loading of the mechanophore in the polyurethane design, with a lower molecular weight PTHF (650 g mol^{-1} instead of 2000 g mol^{-1}) and lack of butanediol chain extender in the case of 1,2-dioxetane. Furthermore, a higher loading (4.5 mol%) of 1,2-dioxetane mechanophore was employed, and the polyurethanes produced were significantly lower in molecular weight (max. 43 kDa).[55] This final formulation achieved higher stress and strain at break than **PU$_L$-AM-1**. All these elements suggest that **AM** activation in polyurethanes can possibly be achieved by introducing the mechanophore within the hard segments, increasing the **AM** loading, and altering the polyurethane design.

Intermolecular hydrogen bonding (H-bonding) interactions are another important element to consider in polyurethanes, as they serve as physical cross-links and provide the inherent toughness of this class of polymers.[55] The strength and density of H-bonding interactions also influence the transfer of macroscopic force onto the mechanophore.[55,69] Under applied tensile stress, the H-bonds are disrupted prior to the activation of the mechanophores.[70] Building on this concept, polyurethane formulations comprising ureidopyrimidinone (UPy) H-bonding supramolecular motifs have been investigated.[65,70,71] The UPy motifs phase-separate into hard domains in these UPy-functionalised polyurethanes, which results in enhanced chain orientation and strain-induced crystallisation of soft segments under tensile strain.[65] These two properties consequently increased the load transfer to spiropyran mechanophores, ultimately enhancing their mechanochemical activation.[70,71] The lower activation force of spiropyrans compared to **AM** does not guarantee that a similar approach would work for **AM**. Thorough computational studies might shed light on principal design aspects to optimise for enabling sufficient force transduction onto mechanophores that have not yet been reported to activate in bulk thermoplastic polyurethanes.[72,73] Nonetheless,

we speculate that further judicious design of hard/soft segment content could provide effective solid-state activation of **AM** units in this matrix.

Finally, we must draw attention to the fact that the synthetic strategies used to obtain **PU_L-AM-1**, **PMA_L-AM-2**, **PMA_N-AM-3**, and **$PDMS_N$-AM-4** result in differing chemical nature of the linking unit between the **AM** and the polymer matrix. The type of linker present has been shown to impact the rupture force of mechanophores.[74] **PMA_L-AM-2**, **PMA_N-AM-3**, and **$PDMS_N$-AM-4** are all connected to the mechanophore *via* the alkoxy side of an ester group, yet only **PMA_N-AM-3** is mechanically active in bulk studies. This would suggest that considerations on the general ductility, strength, stress distribution in the host material, and location of the mechanophore take priority over the linker composition.

Conclusions

In conclusion, we have investigated the ability of the **AM** moieties to undergo the force-mediated retro-Diels–Alder process in various polymer matrices of different toughness and extensibility, in which the mechanophores were either incorporated in the backbone or as cross-links. Our experiments show that the successful activation of the **AM** mechanophores depends strongly on the nature of the polymer matrix, *i.e.*, the molecular topology and perhaps also the mechanical behaviour that it imparts. Strain-rate dependent tensile deformation experiments showed that the activation of the **AM** mechanophores can be achieved in **AM**-centred, linear PMA only at very high strain rates. The work on cross-linked PMA networks suggested that for immediately apparent and strain-rate-independent mechanochemical activation of the **AM** units throughout a material, the mechanophores should serve as cross-links in networks of sufficient toughness and ductility. In the case of polyurethanes, the matrix itself provides a versatile and modular platform that not only influences the material's mechanical properties but also directly impacts force transduction on a molecular scale. We speculate that it should be possible to activate **AM** units in polyurethanes in the solid state by fine-tuning the location of the mechanophore and the strength/density of intermolecular H-bonding interactions. In the case of weak, cross-linked elastomers such as PDMS, reinforcement through interpenetrated network formation may yield materials capable of transducing sufficient stress upon the **AM** units. **AM** has a significantly large activation force as far as reported mechanophores are concerned, which limits suitable host matrices in which it could serve as a force sensor. Finally, we emphasise that while ultrasonication of dilute polymer solutions provides valuable insight for establishing (new) molecular designs as mechanophores, such knowledge may not necessarily translate into comparable activity in bulk materials.

Experimental

PU_L-AM-1

PolyTHF (PTHF) (2 g, 2000 g mol^{-1}) was placed in a 2-necked round-bottom flask with a stirring bar. The flask was kept under vacuum overnight at 80 °C, after which the temperature was decreased to 45 °C. **AM-1** (15 mg, 0.0432 mmol) was placed in a vial, and anhydrous THF (10 mL) was added. The solution was added to the flask containing PTHF by syringe (while kept at 45 °C). Methylene diphenyl diisocyanate (910 mg, 3.64 mmol) was weighed in a vial and dissolved in anhydrous THF (10 mL). This solution was added to the flask containing PTHF and **AM-1** by a syringe (while kept at 45 °C). Dibutyl tin dilaurate (3 drops) was added, and the mixture was stirred for 2 hours at 45 °C. Finally, butanediol (200 μL, 2.26 mmol, kept over molecular sieves) was added to the reaction mixture, and the solution was allowed to stir for 2 hours at 45 °C. The reaction was quenched with ethanol (2 mL). THF (10 mL) was added to dilute the mixture. The quenched reaction mixture was poured into excess methanol to favour precipitation. The polymer was allowed to dry under air, and then it was redissolved in THF (30 mL). The solution was poured into a poly(tetrafluoroethylene) Petri dish and dried over several days. This resulted in 2.92 g (94%) of a polymer film.

PMA_L-AM-2

$Cu^{(0)}$-wire was ground with sandpaper, immersed in 1 M HCl for 15 minutes to remove any copper oxide species, and washed with acetone. Prior to polymerisation, methyl acrylate was passed over basic alumina to remove inhibitors. Bis-functional ATRP initiator **AM-2** (16 mg, 0.024 mmol) and deinhibited methyl acrylate (2.2 mL, 24 mmol) were dissolved in DMSO (1 mL) in a scintillation vial equipped with a pierceable membrane. The $Cu^{(0)}$-wire was wrapped around a magnetic stirring bar and submerged into the reaction mixture in the scintillation vial. The reaction mixture was sparged with N_2 gas for 20 minutes before adding Me6TREN (26 μL, 0.097 mmol). The reaction was allowed to stir at room temperature for 2 hours. The highly viscous solution was poured into H_2O/MeOH to precipitate out **PMA_L-AM-2**, yielding 1.8 g (86%) of polymer. The polymer was redissolved in chloroform and passed over a silica plug to remove residual copper complex species. The filtered polymer solution was poured into a PTFE Petri dish and allowed to air dry to yield polymer films.

PMA_N-AM-3

Irgacure 2959 (1.5 mg; 0.00446 mmol) and **AM-3** diacrylate mechanophore (6.0 mg; 0.132 mmol) were placed in a vial with methyl acrylate (1 mL, 11 mmol). The mixture was sparged with N_2 for 1 minute. Two glass microscope slides were covered carefully with clear tape. Two pieces of parafilm were cut and folded and used as spacers to separate the glass slides. The slides were then clamped together with office clamps, and the solution was added to the gap with a Pasteur pipette. This was immediately irradiated with 365 nm light until the polymerisation was complete. The glass slides were separated. The polymer film was removed and then air-dried over several days.

$PDMS_N$-AM-4

Sylgard® 184 prepolymer base (2 g) was weighed into a beaker and dissolved in THF (20 mL). **AM-4** (14.9 mg; 0.0292 mmol) was

weighed in a vial and dissolved in THF (1 mL). The **AM-4** solution was added to the THF Sylgard® 184 prepolymer solution and stirred until a homogeneous dispersion was obtained. In a separate vial, Sylgard® 184 curing agent (200 mg) was dissolved in THF (2 mL) and then added to the prepolymer/**AM-4** beaker while stirring. The resulting mixture was stirred for 10 minutes. The contents of the beaker were poured into a 10 cm diameter Teflon dish and allowed to dry and cure for 24 hours.

Incorporation of AM-4 into PDMS verification

To verify that the **AM** mechanophore had been successfully incorporated into the PDMS network, the obtained films were submerged and swollen in THF in a 20 mL scintillation vial. The PDMS network was kept in THF overnight, after which the PDMS film was removed, followed by removing the THF *in vacuo*. The recovered residue was then analysed by ^{1}H NMR to determine whether any **AM** had leached out.

Ultrasonication experiments

The experiments were conducted using a Branson Digital Sonifier 450 equipped with a tapered microtip (1/2″/13 mm diameter). Polymer solutions in THF (2 mg mL^{-1}) were introduced to a 25 mL Suslick cell and purged with argon for 10 minutes. The distance between the tip and bottom of the Suslick cell was 1 cm. Temperature control was facilitated by immersing the Suslick cell into an ice bath. The sonication probe was set at 25% amplitude and 1.0 s on and 1.0 s off. The total time for experiments was 300 minutes (150 minutes effective sonication time). Aliquots (1 mL) were taken at regular time intervals and directly used for fluorescence and SEC measurements (in that order).

Ultrasonication experiments on model compound **AM-4** were performed on 15 μg mL^{-1} THF solutions to mirror the amount of **AM** mechanophores present in the experiments on the linear polymers. The sonication probe was set at 25% amplitude, 1.0 s on and 1.0 s off. The total effective sonication time was 150 minutes.

Size-exclusion chromatography (SEC)

Size-Exclusion Chromatography (SEC) experiments were performed on an Agilent 1200 series HPLC system equipped with an Agilent PLGel mixed guard column (particle size = 5 μm) and two Agilent PLGel mixed-D columns (ID = 7.5 mm, L = 300 mm, particle size = 5 μm). Samples were run using THF as the eluent at 30 °C at a flow rate of 1.0 mL min^{-1}. Signals were recorded by a UV detector (Agilent 1200 series) and a differential refractometer (Agilent 1260 RID). Molecular weights were determined based on narrow molecular weight poly(methyl methacrylate) calibration standards.

Tensile testing

Tensile tests were conducted on a Zwick/Roell Z010 (Ulm, Germany) equipped with a 200 N Xforce HP load cell following ASTM D882 standards. For **PMA$_L$-AM-2**, **PMA$_N$-AM-3**, and **PDMS$_N$-AM-4**, rectangular-shaped samples (length: 40 mm, width: 5.35 mm, thickness: 0.25–0.3 mm) were measured at a strain rate of 125% min^{-1} (=2% s^{-1}). For **PU$_L$-AM-1**, dogbone-shaped samples with a length of 40 mm, width of 5 mm, and height of 0.18 mm were measured at a strain rate of 125% min^{-1}. The data reported are averages of three independent measurements, and all errors are standard deviations, reported as the variance in a set of samples compared to the mean of the measurement. Films of identical dimensions were used for the tensile tests at increased strain rates (2500% min^{-1} = 42% s^{-1}, and 5000% min^{-1} = 84% s^{-1}).

Optical characterisation

Fluorescence spectra of polymer solutions were measured with a Horiba Fluorolog 3 spectrometer equipped with a 450 W xenon light source for excitation and an FL-1030-UP photomultiplier as the detector with right-angle (90°) illumination. Fluorescence spectra were recorded with a variable excitation and emission beam slit of 4–14 nm adjusted to record a peak emission intensity of approximately 1.5 × 10^6 counts per second with an excitation wavelength of 350 nm.

In situ fluorescence measurements of solid, as-prepared, and uniaxially deformed polymer samples were measured using an Ocean Optics QE65Pro spectrometer equipped with an LLS-365 LED light source with an excitation wavelength (λ_{ex}) of 365 nm and an Ocean Optics QP230-2-XSR optical fibre (230 μm core) with a measurement spot size of approximately 200 μm. Photographs of the polymer samples were taken under illumination with Phillips UV tube lamps (365 nm, 8 W) inside a black box.

Data availability

The data supporting this article have been included as part of the ESI.†

Conflicts of interest

There are no conflicts to declare.

Acknowledgements

The authors acknowledge funding from the Office of Naval Research (ONR) Global (grant no. N629092212036). All authors thank the Adolphe Merkle Foundation for its generous support.

Notes and references

1 J. Li, C. Nagamani and J. S. Moore, *Acc. Chem. Res.*, 2015, **48**, 2181–2190.
2 D. A. Davis, A. Hamilton, J. Yang, L. D. Cremar, D. Van Gough, S. L. Potisek, M. T. Ong, P. V Braun, T. J. Martínez, S. R. White, J. S. Moore and N. R. Sottos, *Nature*, 2009, **459**, 68–72.
3 H. Chen, F. Yang, Q. Chen and J. Zheng, *Adv. Mater.*, 2017, **29**, 1606900.
4 S. He, M. Stratigaki, S. P. Centeno, A. Dreuw and R. Göstl, *Chem.–Eur. J.*, 2021, **27**, 15889–15897.

5 T. Zeng, L. A. Ordner, P. Liu and M. J. Robb, *J. Am. Chem. Soc.*, 2024, **146**, 95–100.
6 A. Piermattei, S. Karthikeyan and R. P. Sijbesma, *Nat. Chem.*, 2009, **1**, 133–137.
7 S. L. Potisek, D. A. Davis, N. R. Sottos, S. R. White and J. S. Moore, *J. Am. Chem. Soc.*, 2007, **129**, 13808–13809.
8 G. R. Gossweiler, G. B. Hewage, G. Soriano, Q. Wang, G. W. Welshofer, X. Zhao and S. L. Craig, *ACS Macro Lett.*, 2014, **3**, 216–219.
9 M. B. Larsen and A. J. Boydston, *J. Am. Chem. Soc.*, 2014, **136**, 1276–1279.
10 M. M. Caruso, D. A. Davis, Q. Shen, S. A. Odom, N. R. Sottos, S. R. White and J. S. Moore, *Chem. Rev.*, 2009, **109**, 5755–5798.
11 M. Rubinstein and R. H. Colby, in *Polymer Physics*, Oxford University Press, Oxford, 2003, pp. 361–422.
12 C. M. Kingsbury, P. A. May, D. A. Davis, S. R. White, J. S. Moore and N. R. Sottos, *J. Mater. Chem.*, 2011, **21**, 8381–8388.
13 G. I. Peterson and T.-L. Choi, *Chem. Commun.*, 2021, **57**, 6465–6474.
14 M. N. Silberstein, K. Min, L. D. Cremar, C. M. Degen, T. J. Martinez, N. R. Aluru, S. R. White and N. R. Sottos, *J. Appl. Phys.*, 2013, **114**, 023504.
15 I. M. Klein, C. C. Husic, D. P. Kovács, N. J. Choquette and M. J. Robb, *J. Am. Chem. Soc.*, 2020, **142**, 16364–16381.
16 Y. Chen, G. Mellot, D. van Luijk, C. Creton and R. P. Sijbesma, *Chem. Soc. Rev.*, 2021, **50**, 4100–4140.
17 N. Deneke, M. L. Rencheck and C. S. Davis, *Soft Matter*, 2020, **16**, 6230–6252.
18 B. H. Bowser and S. L. Craig, *Polym. Chem.*, 2018, **9**, 3583–3593.
19 X. Hu, M. E. McFadden, R. W. Barber and M. J. Robb, *J. Am. Chem. Soc.*, 2018, **140**, 14073–14077.
20 R. Stevenson and G. De Bo, *J. Am. Chem. Soc.*, 2017, **139**, 16768–16771.
21 X. Hu, T. Zeng, C. C. Husic and M. J. Robb, *J. Am. Chem. Soc.*, 2019, **141**, 15018–15023.
22 J. Kida, K. Imato, R. Goseki, D. Aoki, M. Morimoto and H. Otsuka, *Nat. Commun.*, 2018, **9**, 3504.
23 H.-Y. Duan, Y.-X. Wang, L.-J. Wang, Y.-Q. Min, X.-H. Zhang and B.-Y. Du, *Macromolecules*, 2017, **50**, 1353–1361.
24 S. J. Bailey, C. W. Barney, N. J. Sinha, S. V. Pangali, C. J. Hawker, M. E. Helgeson, M. T. Valentine and J. Read de Alaniz, *Mater. Horiz.*, 2022, **9**, 1947–1953.
25 R. W. Barber, M. E. McFadden, X. Hu and M. J. Robb, *Synlett*, 2019, **30**, 1725–1732.
26 M. B. Larsen and A. J. Boydston, *J. Am. Chem. Soc.*, 2013, **135**, 8189–8192.
27 M. Stratigaki, C. Baumann and R. Göstl, *Macromolecules*, 2022, **55**, 1060–1066.
28 J. Slootman, V. Waltz, C. J. Yeh, C. Baumann, R. Göstl, J. Comtet and C. Creton, *Phys. Rev. X*, 2020, **10**, 41045.
29 E. Izak-Nau, D. E. Demco, S. Braun, C. Baumann, A. Pich and R. Göstl, *ACS Appl. Polym. Mater.*, 2020, **2**, 1682–1691.
30 X. P. Morelle, G. E. Sanoja, S. Castagnet and C. Creton, *Soft Matter*, 2021, **17**, 4266–4274.
31 J. Li, T. Shiraki, B. Hu, R. A. E. Wright, B. Zhao and J. S. Moore, *J. Am. Chem. Soc.*, 2014, **136**, 15925–15928.
32 C. P. Kabb, C. S. O'Bryan, C. D. Morley, T. E. Angelini and B. S. Sumerlin, *Chem. Sci.*, 2019, **10**, 7702–7708.
33 A. R. Sulkanen, J. Sung, M. J. Robb, J. S. Moore, N. R. Sottos and G. Liu, *J. Am. Chem. Soc.*, 2019, **141**, 4080–4085.
34 J. Sung, M. J. Robb, S. R. White, J. S. Moore and N. R. Sottos, *J. Am. Chem. Soc.*, 2018, **140**, 5000–5003.
35 C. Broschinski, F. Majer, S. He, A. J. C. Kuehne and R. Göstl, *ACS Appl. Opt. Mater.*, 2024, **2**, 1764–1769.
36 D. Yildiz, C. Baumann, A. Mikosch, A. J. C. Kuehne, A. Herrmann and R. Göstl, *Angew. Chem., Int. Ed.*, 2019, **58**, 12919–12923.
37 R. Göstl and R. P. Sijbesma, *Chem. Sci.*, 2016, **7**, 370–375.
38 C. Baumann, M. Stratigaki, S. P. Centeno and R. Göstl, *Angew. Chem., Int. Ed.*, 2021, **60**, 13287–13293.
39 M. Stratigaki, C. Baumann, L. C. A. van Breemen, J. P. A. Heuts, R. P. Sijbesma and R. Göstl, *Polym. Chem.*, 2020, **11**, 358–366.
40 X. Hu, T. Zeng, C. C. Husic and M. J. Robb, *ACS Cent. Sci.*, 2021, **7**, 1216–1224.
41 M. Stratigaki, C. Baumann and R. Göstl, *Macromolecules*, 2022, **55**, 1060–1066.
42 C. Baumann, M. Stratigaki, S. P. Centeno and R. Göstl, *Angew. Chem., Int. Ed.*, 2021, **60**, 13287–13293.
43 T. Xie, Z. Li, Y. Zhou, B. Xi and Y. Li, *Macromolecules*, 2024, **57**, 3416–3422.
44 S. M. Luo, R. W. Barber, A. C. Overholts and M. J. Robb, *ACS Polym. Au*, 2023, **3**, 202–208.
45 C. Baumann, N. Willis-Fox, D. Campagna, E. Rognin, P. Marten, R. Daly and R. Göstl, *J. Polym. Sci.*, 2022, **60**, 3128–3133.
46 J. Li, B. Hu, K. Yang, B. Zhao and J. S. Moore, *ACS Macro Lett.*, 2016, **5**, 819–822.
47 G. I. Peterson, J. Lee and T.-L. Choi, *Macromolecules*, 2019, **52**, 9561–9568.
48 N. H. Nguyen and V. Percec, *J. Polym. Sci., Part A: Polym. Chem.*, 2011, **49**, 4241–4252.
49 C. E. Diesendruck, L. Zhu and J. S. Moore, *Chem. Commun.*, 2014, **50**, 13235–13238.
50 M. Di Giannantonio, M. A. Ayer, E. Verde-Sesto, M. Lattuada, C. Weder and K. M. Fromm, *Angew. Chem., Int. Ed.*, 2018, **57**, 11445–11450.
51 S. Jiang, L. Zhang, T. Xie, Y. Lin, H. Zhang, Y. Xu, W. Weng and L. Dai, *ACS Macro Lett.*, 2013, **2**, 705–709.
52 R. Moučka, M. Sedlačík, J. Osička and V. Pata, *Sci. Rep.*, 2021, **11**, 19090.
53 I. D. Johnston, D. K. McCluskey, C. K. L. Tan and M. C. Tracey, *J. Micromech. Microeng.*, 2014, **24**, 035017.
54 D. Dondi, A. Zeffiro, A. Buttafava, C. Marciano, M. Bianchi and A. Faucitano, *Polym. Degrad. Stab.*, 2013, **98**, 392–407.
55 Y. Chen and R. P. Sijbesma, *Macromolecules*, 2014, **47**, 3797–3805.
56 J. W. Kim, Y. Jung, G. W. Coates and M. N. Silberstein, *Macromolecules*, 2015, **48**, 1335–1342.
57 C. R. Siviour and J. L. Jordan, *Journal of Dynamic Behavior of Materials*, 2016, **2**, 15–32.

58 R. Janissen and G. A. Filonenko, *J. Am. Chem. Soc.*, 2022, **144**, 23198–23204.
59 T. Wang, N. Zhang, J. Dai, Z. Li, W. Bai and R. Bai, *ACS Appl. Mater. Interfaces*, 2017, **9**, 11874–11881.
60 E. Ducrot, Y. Chen, M. Bulters, R. P. Sijbesma and C. Creton, *Science*, 2014, **344**, 186–189.
61 J. M. Clough, C. Creton, S. L. Craig and R. P. Sijbesma, *Adv. Funct. Mater.*, 2016, **26**, 9063–9074.
62 W. Qiu, P. A. Gurr and G. G. Qiao, *Macromolecules*, 2020, **53**, 4090–4098.
63 M. F. Rubner, *Macromolecules*, 1986, **19**, 2129–2138.
64 I. Kimura, H. Ishihara, H. Ono, N. Yoshihara, S. Nomura and H. Kawai, *Macromolecules*, 1974, **7**, 355–363.
65 Y. Chen, H. Zhang, X. Fang, Y. Lin, Y. Xu and W. Weng, *ACS Macro Lett.*, 2014, **3**, 141–145.
66 K. Imato, T. Kanehara, T. Ohishi, M. Nishihara, H. Yajima, M. Ito, A. Takahara and H. Otsuka, *ACS Macro Lett.*, 2015, **4**, 1307–1311.
67 C. K. Lee, D. A. Davis, S. R. White, J. S. Moore, N. R. Sottos and P. V Braun, *J. Am. Chem. Soc.*, 2010, **132**, 16107–16111.
68 C. K. Lee, B. A. Beiermann, M. N. Silberstein, J. Wang, J. S. Moore, N. R. Sottos and P. V Braun, *Macromolecules*, 2013, **46**, 3746–3752.
69 Y. Chen, A. J. H. Spiering, S. Karthikeyan, G. W. M. Peters, E. W. Meijer and R. P. Sijbesma, *Nat. Chem.*, 2012, **4**, 559–562.
70 X. Fang, H. Zhang, Y. Chen, Y. Lin, Y. Xu and W. Weng, *Macromolecules*, 2013, **46**, 6566–6574.
71 H. Zhang, Y. Chen, Y. Lin, X. Fang, Y. Xu, Y. Ruan and W. Weng, *Macromolecules*, 2014, **47**, 6783–6790.
72 Y. Sun, W. J. Neary, X. Huang, T. B. Kouznetsova, T. Ouchi, I. Kevlishvili, K. Wang, Y. Chen, H. J. Kulik, S. L. Craig and J. S. Moore, *J. Am. Chem. Soc.*, 2024, **146**, 10943–10952.
73 S. Zhu, N. Lempesis, P. J. in 't Veld and G. C. Rutledge, *Macromolecules*, 2018, **51**, 1850–1864.
74 S. Kumar and T. Stauch, *RSC Adv.*, 2021, **11**, 7391–7396.